Molecular Cell
Article

# Torque Generation of Kinesin Motors Is Governed by the Stability of the Neck Domain

Melanie Brunnbauer,[1] Renate Dombi,[2] Thi-Hieu Ho,[2] Manfred Schliwa,[2] Matthias Rief,[1] and Zeynep Ökten[1,2,*]
[1]Physik Department E22, Technische Universität München, James-Franck-Strasse, 85748 Garching, Germany
[2]Institute for Cell Biology and Center for Integrated Protein Science Munich, University of Munich, Schillerstrasse 42, 80336 Munich, Germany
*Correspondence: zoekten@ph.tum.de
DOI 10.1016/j.molcel.2012.04.005

## SUMMARY

**In long-range transport of cargo, prototypical kinesin-1 steps along a single protofilament on the microtubule, an astonishing behavior given the number of theoretically available binding sites on adjacent protofilaments. Using a laser trap assay, we analyzed the trajectories of several representatives from the kinesin-2 class on freely suspended microtubules. In stark contrast to kinesin-1, these motors display a wide range of left-handed spiraling around microtubules and thus generate torque during cargo transport. We provide direct evidence that kinesin's neck region determines the torque-generating properties. A model system based on kinesin-1 corroborates this result: disrupting the stability of the neck by inserting flexible peptide stretches resulted in pronounced left-handed spiraling. Mimicking neck stability by crosslinking significantly reduced the spiraling of the motor up to the point of protofilament tracking. Finally, we present a model that explains the physical basis of kinesin's spiraling around the microtubule.**

## INTRODUCTION

To ensure an efficient intracellular transport of cargo, eukaryotic cells developed mechanisms of directed transport. One of these mechanisms involves processive molecular motors, which move along the cytoskeletal filaments over long distances by coupling the ATP hydrolysis to mechanical work. Once attached, processive motors can thus take multiple "steps" on their respective filaments without detaching; conversely, unprocessive motors detach from their filaments after one "step." Directed transport by molecular motors plays essential roles in diverse cellular processes, e.g., ciliary transport, transport of membrane-bound vesicles in the cytoplasm, or chromosome segregation during mitosis.

Numerous members of the myosin, kinesin, and dynein families unidirectionally translocate along their filamentous tracks actin and microtubules. Based on this ability, they are termed linear motors. However, these molecules do not always follow a strict linear path along their track; they are capable of producing force perpendicular to their direction of motion as well. The first molecular motor discovered to generate torque was the single-headed dynein purified from Tetrahymena cilia. In in vitro motility assays, surface-attached dynein motors rotated the microtubules around their axis while translocating them in a linear fashion (Vale and Toyoshima, 1988). Such torsional force in addition to axial force generation was subsequently displayed by representatives from all three superfamilies of molecular motors (Nishizaka et al., 1993; Walker et al., 1990; Yajima and Cross, 2005; Yajima et al., 2008).

Within the kinesin superfamily, different behaviors are observed with respect to torque generating properties. Processive kinesin-1, for example, tracks precisely a single protofilament while stepping along a microtubule (Ray et al., 1993). This means that on a microtubule composed of 13 protofilaments where the protofilament axis is aligned with the microtubule axis, tracking results in a perfectly straight motion. In contrast, the weakly processive mitotic kinesin Eg5 (Valentine et al., 2006) follows a left-handed helical path with a pitch of ~2 μm (i.e., it rotates counter-clockwise, as observed with respect to its walking direction), which coincides neither with a possible supertwist of protofilaments nor with any of the helices of the tubulin lattice (Yajima et al., 2008). Lastly, unprocessive kinesins such as dimeric Ncd or artificially single-headed kinesin-1 or kinesin-5 constructs produce a pronounced left-handed microtubule rotation with a pitch of 0.3 μm (Walker et al., 1990; Yajima and Cross, 2005; Yajima et al., 2008). These findings have led to the proposal that the degree of torque generation might serve as a measure for processivity or lack thereof (Yajima et al., 2008).

The latest addition to the list of torque-generating kinesins is the heteromeric kinesin (kinesin-2 family) of *C. elegans* (Pan et al., 2010). Heteromeric kinesins are unique among double-headed motors in that they combine two distinct catalytic subunits to generate a functional motor. This heterodimeric motor associates C-terminally with the nonmotor subunit KAP (Kinesin Associated Protein) to form a heterotrimer (Vukajlovic et al., 2011; Wedaman et al., 1996; Yamazaki et al., 1996). Interestingly, the kinesin-2 from *C. elegans* pairs an unprocessive subunit, KLP11, with a processive one, KLP20, to constitute a processive motor (Brunnbauer et al., 2010). In apparent agreement with the aforementioned hypothesis (Yajima et al., 2008), the unprocessive subunit KLP11, but not the processive KLP20 subunit, produced torque (Pan et al., 2010). Currently, no molecular mechanism exists to explain how kinesins generate torsional in addition to axial force. Is the propensity to generate

torsional force indeed an indicator of processivity, and is therefore torque generation indeed only observed with unprocessive or weakly processive kinesins? And above all, how is torque produced mechanistically?

So far, all results obtained on kinesin's torque-generating properties are inferred from observations of sliding microtubules on surface-attached motors (Nitzsche et al., 2008; Pan et al., 2010; Ray et al., 1993; Walker et al., 1990; Yajima and Cross, 2005; Yajima et al., 2008). Here, we have employed a laser trap assay (Ali et al., 2002, 2004) that allows the tracking of kinesin motion on suspended microtubules between two trapped beads in solution. This experimental geometry is not only a closer mimic of cargo transport but also provides a direct read-out on the motor's torsional pitch. We applied this assay to a range of heterodimeric kinesin-2 motors involved in distinct transport processes in the cytoplasm as well as in cilia. Unexpectedly, we found that heterodimeric kinesin-2 of diverse organisms display an astonishingly broad range of pitches along their paths on microtubules. Thus, torque generation is not confined to mostly artificial, unprocessive, or weakly processive members of the kinesin family but seems to be a prevalent feature for natural kinesin motors involved in diverse transport processes. To identify the domain(s) that determine such behavior, we generated a series of chimeric constructs using the processive kinesin-2 motors from *C. elegans* and mouse (Brunnbauer et al., 2010; Muthukrishnan et al., 2009). Our dissection reveals that the neck, but not the neck linker or the head domains, dictates the spiraling behavior of a motor. Unequivocal support for this finding comes from experiments where a crosslink between the neck linker and the neck of processive kinesin-1 acts as a molecular switch: tampering with the neck stability by introducing flexible residues leads to strong torque generation; mimicking neck stability by crosslinking constrains the motor's path up to the point of single protofilament tracking. In an equivalent approach, we introduced reactive cysteines into the neck region of the kinesin-2 motor from sea urchin that displays the strongest spiraling around the microtubule. The subsequent crosslinking, which again mimics a stable neck, significantly reduced the motor's propensity to generate torque. Based on the structure of the kinesin-1 motor available at atomic resolution (Kozielski et al., 1997; Sindelar et al., 2002; Sindelar and Downing, 2007), we provide a simple mechanistic model that accommodates the correlation between the structure of the neck and the propensity to generate torque in kinesin-1.

## RESULTS

### Probing the Three-Dimensional Trajectories of Kinesin Motors along Suspended Microtubules

We used a multiple-beam optical tweezers setup to study the path of kinesin motors in an unconstrained geometry that allows the motors to access the entire microtubule surface (Ali et al., 2002, 2004). Individual biotinylated and fluorescently labeled microtubules were suspended between two streptavidin-coated "pillar" beads with 3 μm in diameter, which were trapped approximately 20 μm apart. A third trapping potential was used to capture a smaller "cargo" bead with 1 μm in diameter that was coated with motor molecules. The third trap was used to steer the cargo bead and establish contact with the suspended microtubule. As soon as the motors started walking along the microtubule, the cargo bead was released, and its motion along the microtubule was monitored via bright-field microscopy (Figure 1A). Specifics of the experimental geometry and the data analysis are discussed in the Supplemental Information (Figure S1).

In the first set of experiments, we established the robustness of our experimental geometry using kinesin-1 from *D. melanogaster* (*Dm*KHC) (Figure 1B), which is known to track a single protofilament on the microtubule surface (Nitzsche et al., 2008). When we tested the movement of *Dm*KHC-coated beads on different suspended microtubules, we mainly observed a left-handed spiraling motion of the beads around the microtubule with a mean pitch of 5.7 ± 1.1 μm (mean ± SD, 17 beads tested on 7 different microtubules) (Figures 1C and 1D and Movie S1). This value matches closely the predicted protofilament supertwist of a microtubule composed of 14 protofilaments according to the lattice rotation model (Chrétien and Wade, 1991; Ray et al., 1993). Furthermore, we occasionally detected straight movement or a right-handed spiraling (pitch ~4 μm), which correspond to microtubules built from 13 or 12 protofilaments, respectively (Figure 1D). Taken together, our results are consistent with *Dm*KHC tracking individual protofilaments as demonstrated previously and show that, as expected for the polymerization conditions used here, 14-protofilament microtubules constitute the majority (Ray et al., 1993).

### Heterodimeric Kinesin-2 of Diverse Organisms Display an Astonishing Variability in Their Trajectories on Microtubules

Heteromeric kinesins coevolved with the cilia to work on microtubule doublets and were later adapted for cytoplasmic transport on singlet microtubules (Mitchell, 2007; Scholey, 2003). The neuronal transporter *Mm*KIF3a/3b (Yamazaki et al., 1995) and the melanosome transporter *Xl*KLP3a/3b (Tuma et al., 1998) are the prominent representatives of kinesin-2 motors involved in cytoplasmic transport. Processive movement along microtubules was demonstrated with *Mm*KIF3a/3b, *Xl*KLP3a/3b, and *Ce*KLP11/20 (Brunnbauer et al., 2010; Kural et al., 2007; Muthukrishnan et al., 2009), whereas *Sp*KRP85/95 was reported to be a nonprocessive motor (Pierce et al., 1999).

We probed the transport paths of the aforementioned full-length heterodimeric kinesin-2 motors in our setup. Because the wild-type *Ce*KLP11/20 is an autoinhibited motor, we introduced the corresponding deinhibiting mutations in the conserved region within the stalk (see Supplemental Information and Figure S2A) of all the kinesin-2 motors to circumvent potential experimental problems caused by inhibited motors (Brunnbauer et al., 2010; Imanishi et al., 2006). The trajectories of these different kinesin-2 constructs along suspended microtubules revealed a tremendous variability in their spiraling behavior. Except for *Mm*KIF3a/3b, all heterodimers exhibited a characteristic left-handed spiraling (Figure 2 and Movie S2). Equivalent results were obtained with all constructs containing the wild-type stalk, demonstrating that the deinhibiting mutations do not interfere with the propensity of the motors to generate torque (Figures S2B and S2C). *Sp*KRP85/95 displayed the tightest pitch

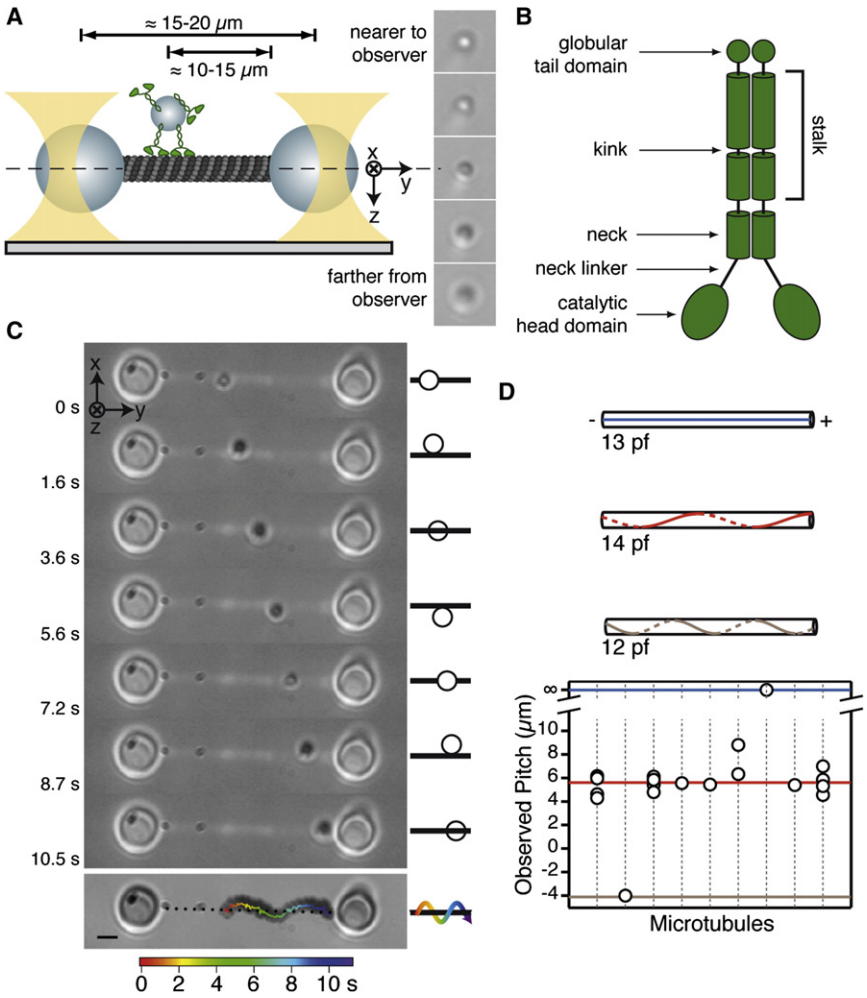


**Figure 1. Probing the Trajectories of Kinesins along Suspended Microtubules**

(A) Schematic representation of the experimental geometry (not to scale). A microtubule (gray) is suspended between two 3 μm "pillar beads" (blue) trapped in two laser foci (yellow). The third laser focus used to place the 1 μm "cargo bead" on the microtubule is not shown. The motion of the cargo bead coated with multiple motor molecules (green) is monitored via bright-field microscopy (bright-field images represent a view from top). Typical distances are indicated. Right: the height of the cargo bead relative to the focal plane (dashed line) can be qualitatively determined by its appearance. Images are taken at z = −1, −0.5, 0, +0.5, and +1 μm.

(B) Domain organization of double-headed kinesin motors. The neck linker links the catalytic head domains to the rest of the protein, which we refer to as the neck-stalk-tail (NST) domains throughout the text. The stalk domain contains the conserved autoinhibitory kink, which allows the tail domain to fold back onto the head domains if the motor is not bound to its cargo.

(C) Motion of a *Dm*KHC-coated bead along a suspended microtubule. The fluorescence image of the microtubule has been superimposed onto the bright-field image for illustration purposes. Sketches on the right represent the position of the bead relative to the microtubule as deduced from the appearance of the cargo bead (A), revealing the left-handedness of the spiraling motion. The bottom image represents a superposition of consecutive bright-field images (frame rate 40 ms) demonstrating the complete path of the bead along with the x-y tracking data of the bead position (rainbow colored line). Scale bar: 2 μm.

(D) Top: depending on the number of protofilaments that build up the wall of the tube-like microtubule structure, the protofilament axis runs parallel to the microtubule axis (13 pf, blue) or describes a shallow left- (14 pf, red) or right-handed (12 pf, brown) helical path on the microtubule surface. Bottom: measured pitches for individual *Dm*KHC-coated beads (circles) on different microtubules (dashed lines). Colored lines indicate expected supertwists for microtubules composed of 12, 13, and 14 protofilaments.

among the heterodimeric kinesins, followed by the processive *Ce*KLP11/20 and *Xl*KLP3a/3b motors (see Supplemental Information for a detailed discussion on the superimpositions of the motor's pitch with the microtubule's supertwist [Figures S2C and S2D]). The processive *Mm*KIF3a/3b heterodimer from mouse was in fact the only kinesin-2 motor in our study that displayed close protofilament tracking as observed with the kinesin-1. Taken together, the ability to spiral around the microtubule does not originate from the presence of two distinct heads, nor does it unequivocally correlate with the motor's processivity. For example, the heterodimeric motors from *C. elegans* and mouse are similarly processive (Brunnbauer et al., 2010; Muthukrishnan et al., 2009); however, the former displays considerable torque while the latter moves torque-free.

The analysis of *Ce*KLP11/20 and its previously characterized chimeras (Brunnbauer et al., 2010) is consistent with the conclusions drawn from the spiraling behavior of diverse representatives of the kinesin-2 class: the processive *Ce*KLP11/20 displays an equivalent spiraling compared with the unprocessive KLP11/11 and the processive KLP20/20 "homodimeric" chimeras (Figure 3, Figure S3, and Movie S3). The spiraling of the *Ce*KLP11/20 and its chimeric KLP20/20 homodimer are in apparent discrepancy with previously published results in which no spiraling of the constructs was observed with surface-attached motors (Pan et al., 2010). This might be due to the differences in the sensitivity of the readout (rotating microtubule versus spiraling cargo bead) between the respective experimental setups.

Our attempts to determine the pitch of single-motor molecules were hampered due to the 4- to 5-fold decrease in run length displayed by kinesin-2 motors compared to kinesin-1 (Brunnbauer et al., 2010; Muthukrishnan et al., 2009). As a consequence, the probability of observing a run length of merely 2 μm with single *Mm*KIF3a/3b or *Ce*KLP11/20 dimers is below 1%. However, previous experiments with kinesin-1 showed no influence of the motor density on the torque generation properties (Ray et al., 1993).

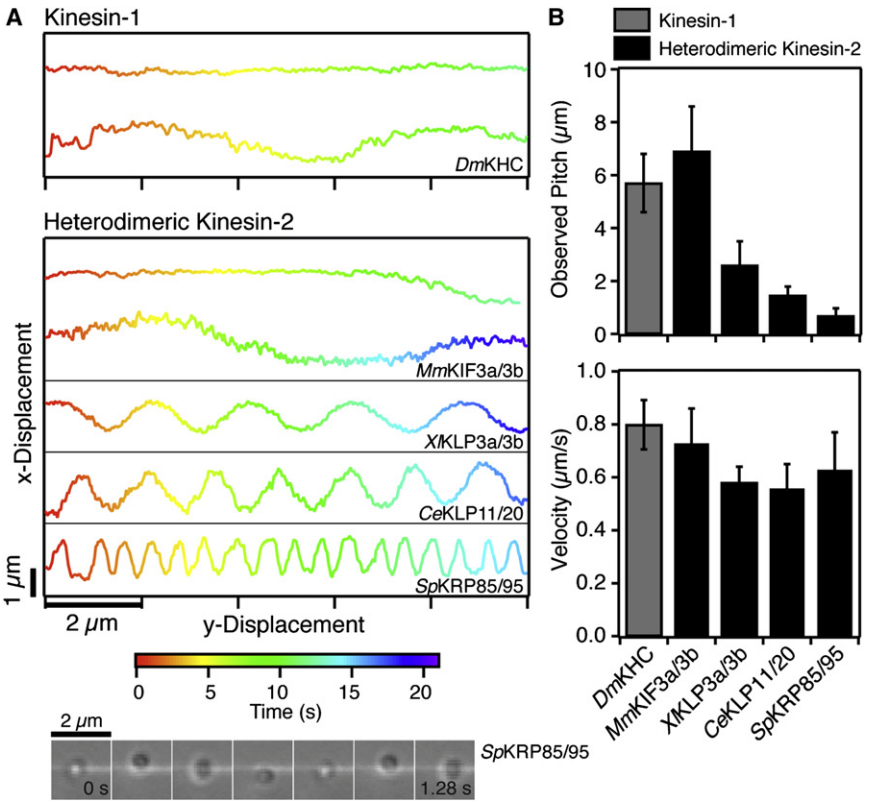


**Figure 2. Heterodimeric Kinesin-2 Motors Display a High Variability in Their Path along Microtubules**

(A) Representative x-y traces of different kinesin-2 motors. Upper panel: the kinesin-1 *Dm*KHC displays no or shallow spiraling around microtubules, reflecting the supertwist of protofilaments in the microtubule (top trace, 13 pf; bottom trace, 14 pf). Lower panel: heterodimeric kinesin-2 motors from diverse organisms differ considerably in their spiraling behavior around the microtubule.

(B) Observed pitches for left-handed spiraling (p) given as mean ± SD for the different kinesins. *Mm*KIF3a/3b: p = 6.9 ± 1.7 μm, n = 14, N = 5; *Xl*KLP3a/3b: p = 2.6 ± 0.9 μm, n = 30, N = 12; *Ce*KLP11/20: p = 1.5 ± 0.4 μm, n = 28, N = 14; *Sp*KRP85/95: p = 0.7 ± 0.3 μm, n = 38, N = 16 (n, number of beads; N, number of microtubules). Velocities of the respective motors are given as mean ± SD.

## Neither the Head Domain nor the Neck Linker Control Torque Generation in Kinesin-2

In an attempt to identify the domain(s) that dictate the spiraling behavior of kinesins, we generated a series of chimeric constructs using the processive kinesin-2 motors *Ce*KLP11/20 and *Mm*KIF3a/3b from *C. elegans* and mouse, respectively. The former displays a left-handed pitch of 1.4 μm, while the latter tracks the supertwist of the microtubule (Figure 2). Specifically, we screened the individual contributions of the head domain, the neck linker (nl), and the remaining nonmotor domains (neck, stalk, and tail, or NST, Figure 1B) to the torque-generating behavior in the kinesin motor. Figure 4 shows the splice sites used to generate the respective constructs.

Replacing the neck linker and the NST of *Mm*KIF3a/3b with the corresponding domains of *Ce*KLP11/20 results in left-handed spiraling of the motor (Figure 4B, first trace, Figure S4A, and Movie S4, first panel). This indicates that not the head domains but the neck linker and/or the NST determine the torque production of the motor molecule. Resubstitution of the KIF3a/3b NST domains reduces torque generation dramatically, indicating that the spiraling of the motor is induced by domains located C-terminally to the neck linker (Figure 4B, second trace, Figure S4A, and Movie S4, second panel). Indeed, solely replacing the NST domains of *Mm*KIF3a/3b with *Ce*KLP11/20 generates a spiraling behavior equivalent to *Ce*KLP11/20 (Figure 4B, third trace, Figure S4A, and Movie S4, third panel). Taken together, this indicates that the functional determinants of torque generation are not located in the catalytic heads or the neck linker, but in the NST domains.

Our efforts to cross-check this finding by determining the torque generation properties of an inverse heterodimeric chimera with the head domains from the *C. elegans* kinesin-2 and NST domains from mouse kinesin-2 were impeded by the lack of expression of the chimeric subunit KLP20(head+nl)-KIF3a(NST). However, we succeeded in generating a chimeric motor, in which the head domain and neck linker of the KIF3b subunit of *Mm*KIF3a/3b were substituted by the corresponding elements of KLP11 (Figure S4B). This chimera combines catalytic domains of two distinct kinesin-2 motors with equal processivity but different spiraling behavior. The spiraling behavior of this construct was experimentally indistinguishable from the construct KIF-KLP(nl) (Figure 4B, second trace, Figure S4B, and Movie S4, fourth panel). Thus, introducing a catalytic head (KLP11) displaying a strong propensity to generate torque in its wild-type context does not impose spiraling to the protofilament-tracking motor *Mm*KIF3a/3b, in line with our previous results.

Our mechanistic dissection consistently identifies the region C-terminal to the neck linker to contain the torque generating element. To further narrow down the region responsible for torque generation in kinesin-2, we have swapped the polypeptide stretches between the *Mm*KIF3a/3b and *Ce*KLP11/20 heterodimers using the experimentally confirmed splice sites marking the end of the neck linker (Brunnbauer et al., 2010; Muthukrishnan et al., 2009) and the universally conserved kink region containing the flexible glycine residues. The resulting *Mm*KIF3a/3b chimeric construct containing the extended neck region of the *Ce*KLP11/20 heterodimer displayed pronounced spiraling around the microtubule, equivalent to the *Ce*KLP11/20 heterodimer (Figure 4B, fourth trace, Figure S4A, and Movie S4, fifth panel). We therefore conclude that the structural element responsible for torque generation in kinesin-2 is situated C-terminal to the neck linker and N-terminal to the kink.

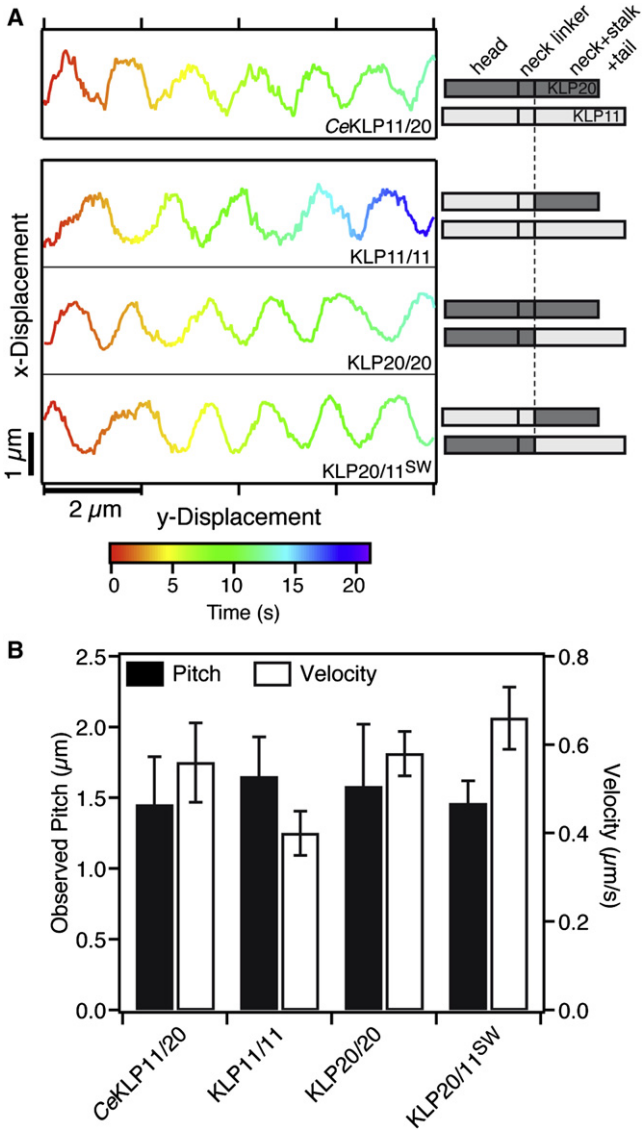


**Figure 3. Torque Generation in Kinesin-2 Is Not the Result of Combination of the Two Distinct Head Domains**

(A) x-y traces for heterodimeric kinesin *Ce*KLP11/20 and its chimeric constructs. The design of the chimeric constructs with identical or swapped head domains is shown on the right.

(B) Measured pitches for left-handed spiraling (p) are given as mean ± SD (black bars). *Ce*KLP11/20: p = 1.5 ± 0.4 μm, n = 28, N = 14; KLP11/11: p = 1.7 ± 0.3 μm, n = 11, N = 3; KLP20/20: p = 1.6 ± 0.5 μm, n = 12, N = 2; KLP20/11$^{SW}$: p = 1.5 ± 0.2 μm, n = 10, N = 2 (n, number of beads; N, number of microtubules). Velocities in y-direction are given as mean ± SD (white bars).

## The Neck Dictates the Torque-Generating Properties of Double-Headed Kinesins

As we narrowed down the location of the torque-conferring element to be between the neck linker and the kink, we hypothesized that the neck is a likely candidate region for the motor's capability to switch protofilaments and thus spiral around the microtubule. Our working hypothesis states that an unstable neck region increases the reach of the two kinesin head domains and thus allows the motor to switch protofilaments and spiral around the microtubule. Conversely, constraining the reach of the head domains should coerce the motor to follow the protofilament.

To test this hypothesis, we analyzed a functionally characterized human kinesin-1 cysteine-light construct and a mutant derived from it that contains flexible glycine-serine (GS) extensions between the neck linker and neck (Rice et al., 1999; Yildiz et al., 2008). To reversibly control the reach of the two head domains, we engineered a reactive cysteine (KKCK) between the neck linker and the flexible GS motif (Figure 5A) (Okten et al., 2004; Rice, 2001). Specific crosslinking of the introduced cysteines mimics a stable neck region and was accomplished by a bis-functional cysteine-reactive crosslinker. A control kinesin-1 dimer where the reactive cysteine is replaced with a glycine residue (KKGK) was subjected to the same procedure and confirmed that the cysteine crosslinking is specific (Figure 5B).

As predicted, the crosslinking of the cysteine residues acted as a molecular switch for the motor's torque-generating ability (Figures 5C and 5D). The tracking of one protofilament by kinesin-1 containing the wild-type neck (Figure 5C, upper traces, Figure S5, left panel, and Movie S5, first and second panels) switched to a pronounced left-handed spiraling when a flexible insert disrupted the stability of the wild-type neck coiled coil (Figure 5C, middle trace, Figure S5, middle panel, and Movie S5, third panel). Remarkably, restraining the reach of the head domains by cysteine crosslinking, thereby mimicking neck stability, dramatically reduced the spiraling behavior around microtubules, up to the point of protofilament tracking (Figure 5C, bottom traces, Figure S5, right panel, and Movie S5, fourth panel). It is important to note that the crosslinking reaction is highly efficient but not complete (Figure 5B). Uncrosslinked motors are thus involved in bead transport as well, which might account for the residual degree of torque generation in some trajectories (Figure 5D, left panel, Movie S5, fifth panel). In contrast, the homogenous population of the uncrosslinked construct never showed examples of protofilament tracking and only displayed narrowly distributed tight pitches (Figure 5D, left panel). Consistent with previous observations (Yildiz et al., 2008), crosslinking also rescues the velocities close to wild-type levels (Figure 5D, right panel). We conclude that the stability of the neck region specifies the torque generation properties of kinesin-1 motors.

We wondered if the neck stability also influences the torque-generating properties in kinesin-2 motors. Because no cysteine-light mutant is available for the kinesin-2 motors, we introduced the highly reactive cysteine (KKCK) into the kinesin-2 with the least amount of wild-type cysteines, *Sp*KRP85/95. The engineered reactive cysteines are each located four residues after the conserved splice sites marking the end of the respective neck linkers (Figure 6A). To achieve specific crosslinking, we had to decrease the pH to 6.5 during crosslinking to render the wild-type cysteines less reactive relative to the engineered cysteines that are embedded in a patch of basic lysine residues (Figure 6B). Constraining the neck region of *Sp*KRP85/95 via crosslinking significantly increased the pitch of the spiraling motor, whereas the uncrosslinked construct behaved as the wild-type *Sp*KRP85/95 (Figures 6C and 6D and Movie S6). The molecular switch introduced into the neck region of kinesin-2 controls the

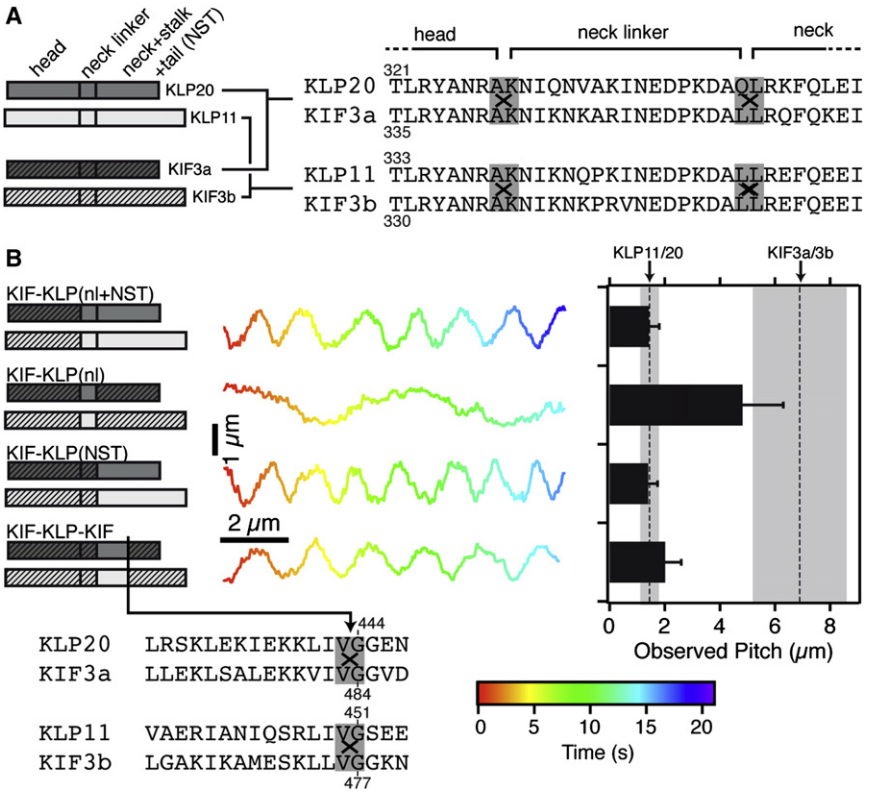


**Figure 4. The Region C-Terminal to the Neck Linker and N-Terminal to the Kink Determines the Propensity to Generate Torque in Heterodimeric Kinesin-2**

(A) Design of the chimeric constructs assembled with the "straight" walking *Mm*KIF3a/3b and the spiraling *Ce*KLP11/20 motors, respectively. The splice sites before and after the neck linker for the corresponding subunits (KIF3a/KLP20 and KIF3b/KLP11) are indicated by gray shades.

(B) x-y traces of the KIF/KLP chimeras. The arrow indicates the splice site at the kink position used to create the KIF-KLP-KIF chimera (bottom panel). The splice site after the neck linker is as shown in (A), top panel. Measured pitches for left-handed spiraling (p) are given as mean ± SD (black bars). KIF-KLP(nl+NST): p = 1.4 ± 0.4 μm, n = 22, N = 8; KIF-KLP(nl): p = 4.8 ± 1.5 μm, n = 27, N = 9; KIF-KLP(NST): p = 1.4 ± 0.4 μm, n = 22, N = 6; KIF-KLP-KIF: p = 2.0 ± 0.6 μm, n = 11, N = 9 (n, number of beads; N, number of microtubules). The average pitches of the *Ce*KLP11/20 and *Mm*KIF3a/3b motors are indicated by dashed lines (±SD, gray shading).

spiraling behavior as demonstrated with kinesin-1 (Figure 5). The crosslinking of the sea urchin kinesin-2 after the neck linker is notably the least artificial construct that tests our hypothesis: this construct contains only four introduced amino acids (per polypeptide, as compared to the wild-type motor protein) to serve as a molecular switch in the motor's neck region. We therefore conclude that our hypothesis can explain the torque generation properties of kinesin-1 as well as kinesin-2 motors.

## A Simple Mechanistic Model for Kinesin's Left-Handed Spiraling

Intriguingly, molecular motors in general display an intrinsic preference in handedness. So far, all spiraling plus-end-directed motors, kinesins and myosins alike, consistently show a left-handed spiraling around their filaments (Ali et al., 2002; Pan et al., 2010; Yajima and Cross, 2005; Yajima et al., 2008). However, the molecular origin for this intrinsic handedness remains elusive.

While our results so far have identified the stability of the neck region as the key determinant for spiraling versus protofilament tracking, the extended reach of the head domains alone cannot explain why spiraling exclusively occurs in a left-handed direction. The bias in the direction of torque generation must reside entirely in the properties of the head domain. The flexible connection between the two head domains in the processive double-headed motor then acts as a switch deciding whether the intrinsic left-handed bias of a single-head domain leads to binding to off-axis binding sites or whether the rebinding head is restrained to the protofilament as it moves on. Based on these considerations, we propose a simple mechanistic model that explains the observed left-handed spiraling of kinesin-1 with a flexible neck (see Supplemental Information for details).

Our starting point for the mechanistic model is the commonly accepted stepping model, in which the forward step is produced by the docking of the neck linker to the leading head. Docking brings the trailing head to the front, followed by a diffusive search for the next binding site (Carter and Cross, 2005; Rice et al., 1999). Our model takes into account that docking of the neck linker (1) shortens the flexible connection of the two heads by the length of the docked portion and (2) shifts the starting point for the diffusive search in the plus end direction of the microtubule. Additionally, we assume a left-handed bias of the starting point, as the power stroke of single-headed kinesin-1 displays a left-handed torque component (Yajima and Cross, 2005). Based on these considerations, we predict the probabilities for reaching potential binding sites on the microtubule lattice by calculating the elastic energy needed to stretch the flexible extension between the two-headed domains.

For kinesin-1, the model predicts consistent protofilament tracking, as shown in Figure 7A. In contrast, for a motor with flexible KKCK$(GS)_7$ inserts, there exist finite probabilities to reach binding sites on neighboring protofilaments, in agreement with the experimentally observed step size distribution (Yildiz et al., 2008) (Figure 7B, left panel). Monte-Carlo simulations of a motor's path using the obtained probabilities reproduce a left-handed spiraling motion around a microtubule (Figure 7B, right panel). The calculated net probability for left-handed sidestepping of 13% results in an estimated pitch of approximately 0.8 μm, which is in good agreement with the measured pitch of this motor (0.71 ± 0.33 μm).

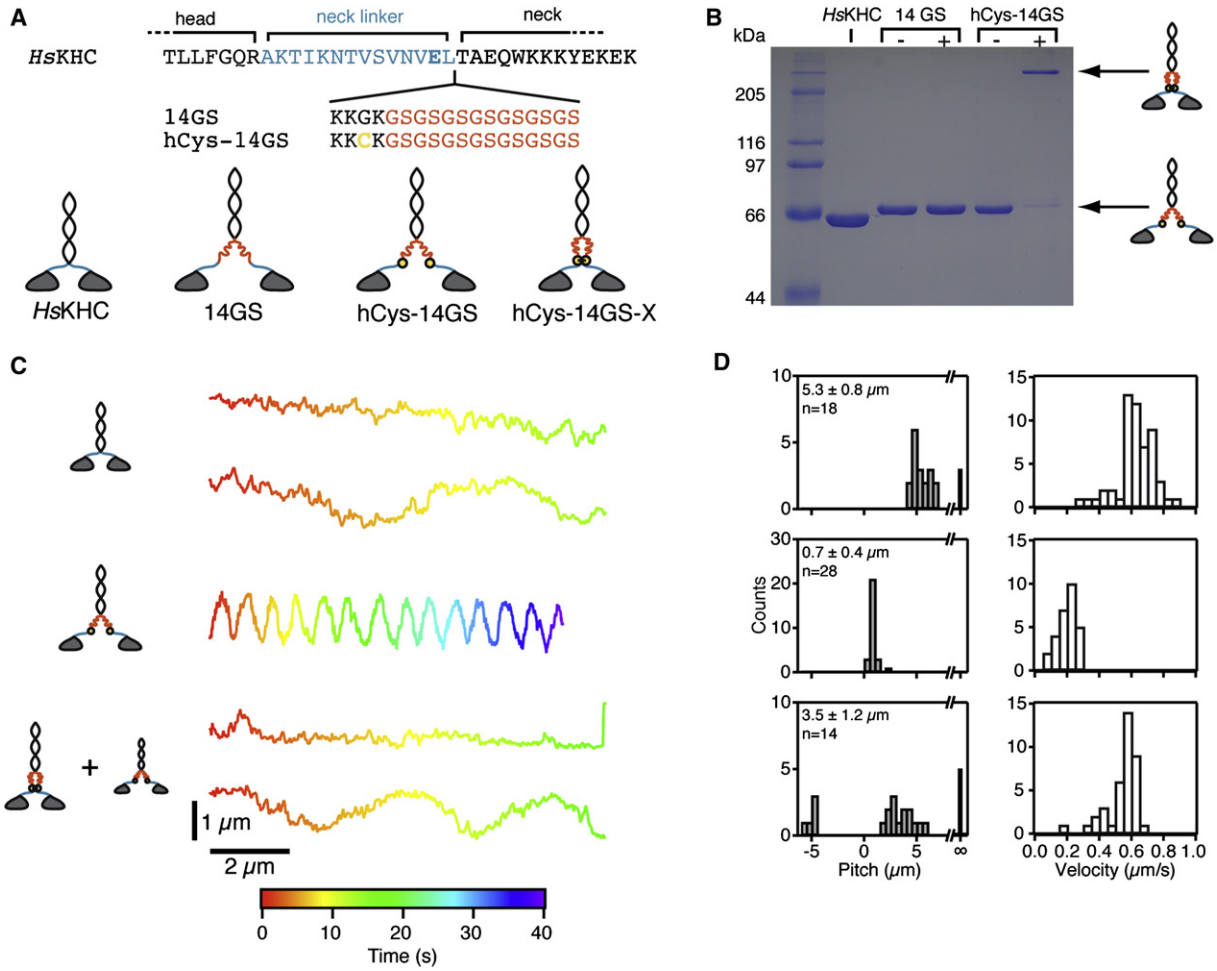


**Figure 5. Engineering a Molecular Switch for Spiraling into Human Kinesin-1**

(A) Design of the human kinesin-1 constructs with flexible necks. The neck linker is shown in cyan; flexible poly-GS inserts are shown in red.

(B) SDS-PAGE analysis of the efficiency and the specificity of the cysteine-cysteine crosslinking reaction with the bis-functional $BM(PEG)_2$ crosslinker. (−, no crosslinker; +, with crosslinker).

(C) x-y traces of the *Hs*KHC, hCys-14GS, and the hCys-14GS-X constructs.

(D) Left: histogram of the observed pitches (mean ± SD) for the kinesin-1 constructs. *Hs*KHC: p = 5.3 ± 0.8 μm, n = 18, N = 8; hCys-14GS: p = 0.7 ± 0.4 μm, n = 28, N = 9; hCys-14GS-X: p = 3.5 ± 1.2 μm, n = 14, N = 6 (n, number of beads; N, number of microtubules). Right: histogram of velocities in the y direction.

In addition, the model predicts a slightly increased tendency for sidestepping of the double-headed motor, including four lysine residues preceding the crosslinking site (Figure 7C). In fact, if this additional flexibility provided by these lysine residues is taken into account, a spiraling with a pitch of 3 μm is predicted on a 14 protofilament microtubule, which closely matches the motor's observed pitch of 3.5 ± 1.2 μm.

## DISCUSSION

The prototypical long-range molecular cargo transporter is the processive kinesin-1 motor. The cargo transport in vivo takes place on microtubules composed of mostly 13 laterally associated protofilaments (Tilney et al., 1973). Despite moving on the surface of a microtubule with many theoretically accessible binding sites, the path of kinesin-1 was shown be restricted to one protofilament (Nitzsche et al., 2008; Ray et al., 1993; Yajima and Cross, 2005). In stark contrast, surface-attached natural or engineered unprocessive kinesins generated pronounced microtubule rotation in in vitro assays (Nitzsche et al., 2008; Ray et al., 1993; Walker et al., 1990; Yajima and Cross, 2005; Yajima et al., 2008). The intermediate rate of rotation displayed recently by a weakly processive kinesin thus intuitively suggested causality between a motor's processivity and its torque-generation properties (Yajima et al., 2008). However, our understanding of torque generation in addition to translational movement by kinesins is so far limited to a few examples. We have set out to mechanistically understand the source of torque generation by kinesins and examine its previously suggested correlation to processivity.

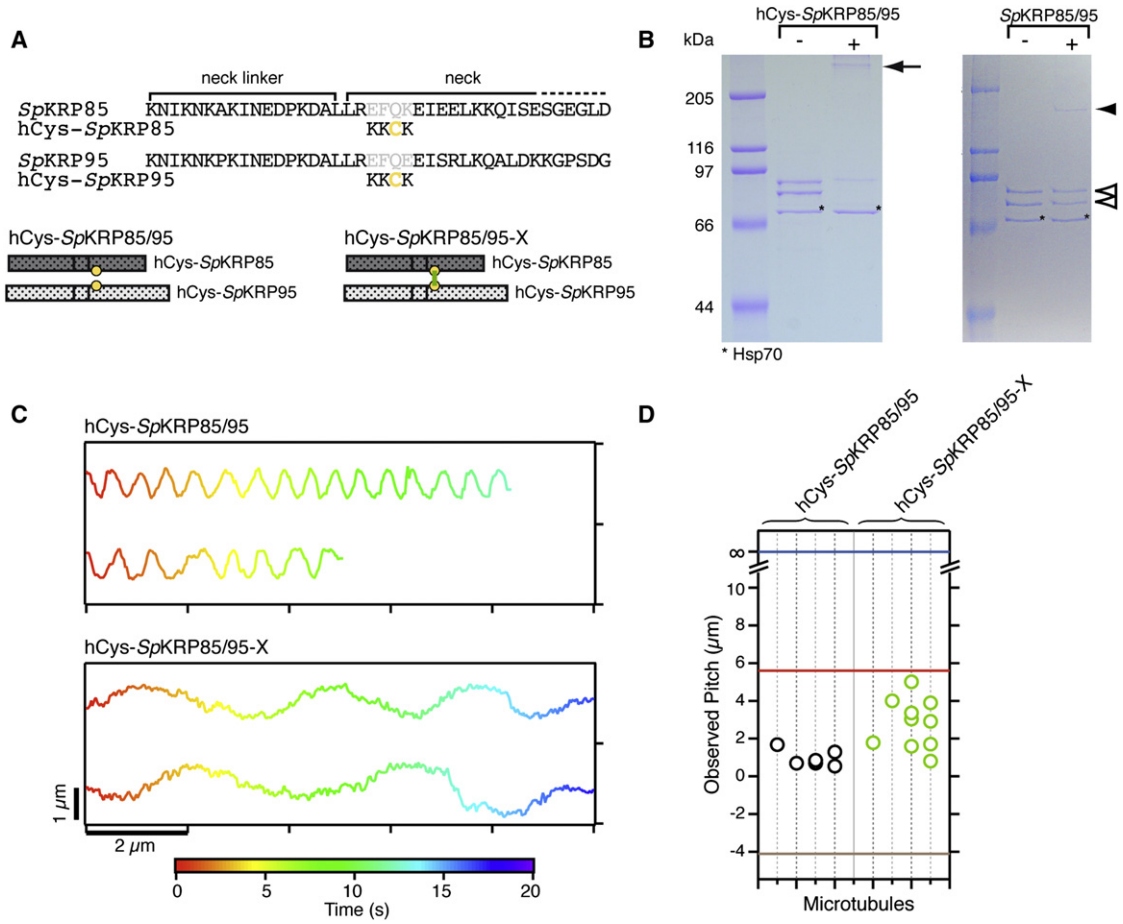


**Figure 6. Manipulating the Spiraling Behavior of *Sp*KRP85/95**

(A) Design of the hCys-*Sp*KRP85/95 constructs to mimic a stable neck via chemical crosslinking. The reactive cysteines are shown in orange.

(B) SDS-PAGE analysis of the efficiency and the specificity of the crosslinking reaction of the hCys-*Sp*KRP85/95 construct containing the reactive cysteines (left panel: −/+ crosslinker) and the *Sp*KRP85/95 control (right panel: −/+ crosslinker), respectively. As expected, the hCys-*Sp*KRP85/95 construct displays a nearly complete crosslinking of the two polypeptide chains (black arrow), whereas the *Sp*KRP85/95 containing only the wild-type cysteines is nearly inert to crosslinking (open arrowheads). The control reaction with the bis-functional $BM(PEG)_2$ crosslinker yields a weak band that results from unspecific crosslinking of the native cysteines (filled arrowhead). This unspecific crosslinking, however, is abolished in the presence of the engineered, reactive cysteines. The presence of both subunits in the crosslinked band of hCys-*Sp*KRP85/95 was confirmed via mass spectrometry analysis (LC-MS/MS).

(C) x-y traces of the hCys-*Sp*KRP85/95 constructs. The top panel shows traces of the hCys-*Sp*KRP85/95 prior to the crosslinking. Bottom traces show the increased pitch of the construct after the crosslinking reaction.

(D) Measured pitches of the hCys-*Sp*KRP85/95 constructs on different microtubules (dashed vertical lines). The respective supertwists of the filaments are indicated in red (14 pf), in blue (13 pf), and in brown (12 pf). Black circles represent the spiraling behavior of beads coated with the uncrosslinked hCys-*Sp*KRP85/95 motor, and the green circles represent the spiraling behavior of the crosslinked hCys-*Sp*KRP85/95-X. hCys-*Sp*KRP85/95: p = 0.9 ± 0.4 μm, n = 7, N = 4; hCys-*Sp*KRP85/95-X: p = 2.8 ± 1.3 μm, n = 10, N = 4 (n, number of beads; N, number of microtubules; values represent mean ± SD). As expected, the crosslinking after the neck linker in *Sp*KRP85/95 kinesin-2 increased the pitch of the motor. Note that in the crosslinked fraction, uncrosslinked motors are evidently still present and interfere with the movement of the bead (green circles displaying pitches equivalent to the uncrosslinked hCys-*Sp*KRP85/95 construct shown in black circles).

In our laser trap assay, kinesin motors can move freely on suspended microtubules, mimicking cargo transport as accurately as possible. In this setup, heterodimeric kinesin-2 motors from diverse organisms displayed an astounding range of rotational pitches, expanding the list of torque-generating kinesins to include processive representatives of the kinesin-2 family. This immediately raises the question of the mechanistic differences within this family of conserved motors and the molecular origin of force generation by kinesins in general.

## Dimerization Properties of Kinesins and Protofilament Switching

Why does the neck-stalk-tail (NST) of the mouse kinesin-2 and kinesin-1 prevent switching protofilaments whereas the NST of *X. laevis* and *C. elegans* kinesin-2 do not? The dimerization properties of the kinesin motors offer the first clues. In a double-headed kinesin, the two catalytic head domains are thought to be joined by a neck via coiled-coil interactions. This has been convincingly demonstrated for the dimeric kinesin-1 from rat at

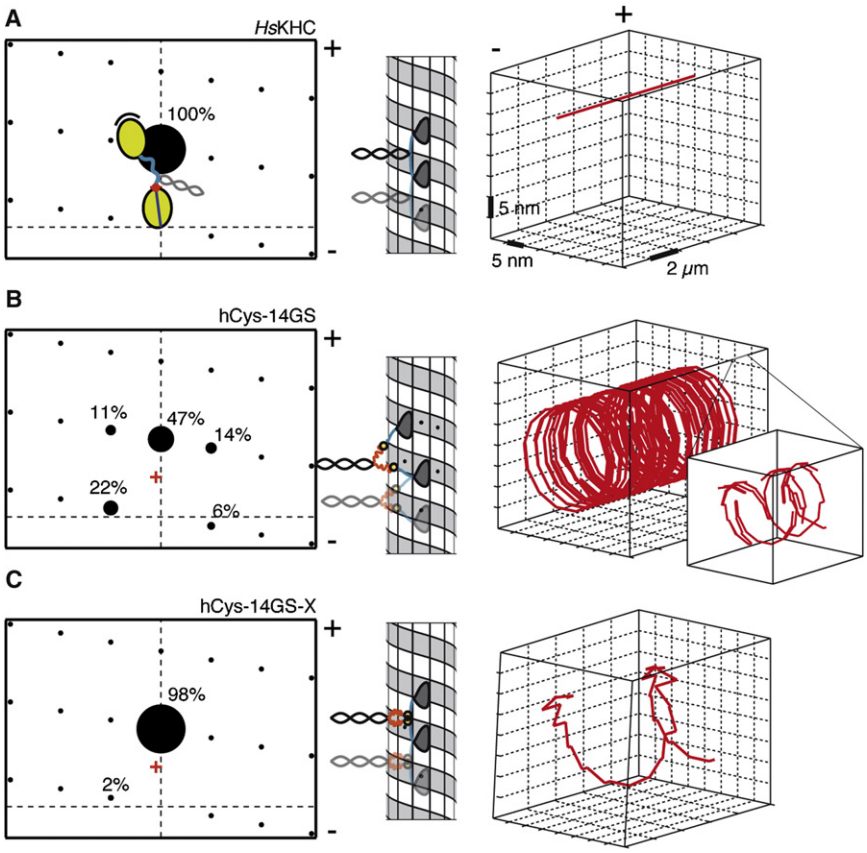


**Figure 7. Mechanistic Model for Kinesin Spiraling**

Diffusive search for the next binding site of *Hs*KHC (L = 10.2 nm) (A), hCys-14GS (L = 23 nm) (B), and hCys-14GS-X (L = 11.7 nm) (C). L: contour length of the flexible connection of the heads. The flexibility of the connection between the head domains influences the probabilities to reach off-axis binding sites (left panels, black markers). The panels on the right illustrate the simulated path of a motor, taking the calculated probabilities into account (plus and minus ends of the microtubule are indicated).

atomic resolution, which revealed a coiled-coil structure immediately following the neck linker (Kozielski et al., 1997). Indeed, extending the head domains of kinesin-1 from human and *D. melanogaster* just by the neck region (~30–40 residues) is sufficient to purify a stable homodimeric motor (Huang et al., 1994; Morii et al., 1997; Tripet et al., 1997). Incidentally, kinesin-1 from human and *D. melanogaster* and the kinesin-2 from mouse all follow one protofilament of the microtubule, as demonstrated in our assay (Figures 1, 2, and 5) and by others (Nitzsche et al., 2008), implicating a stable neck formation in the mouse kinesin-2 as well (Chana et al., 2005). In contrast, *X. laevis* and *C. elegans* kinesin-2 do not form stable dimers autonomously in the neck region, as both require the distal C-terminal part of the stalk to initiate heterodimer formation (De Marco et al., 2001; Vukajlovic et al., 2011). A dimerization "seed" located at the end of the C-terminal stalk is necessary for dimer formation, suggesting a less stable N-terminal neck. Our recent work on the heterodimerization properties of the *C. elegans* kinesin-2 indicates that the N-terminal part of the stalk is indeed less stable than the C-terminal part (Vukajlovic et al., 2011). Interestingly, both kinesin-2 motors spiral around the suspended microtubule. Taken together, neck coil stability seems to determine if a motor is capable of bridging the distance between the protofilaments, which in turn is a prerequisite to spiral around the microtubule. Similarly, flexible elements joining two catalytic heads in the dynein motor were shown to produce side-stepping on the microtubule (Reck-Peterson et al., 2006).

## Kinesin's Neck Stability Controls Protofilament Switching

We have provided direct evidence for the suggestion that neck stability dictates the path of kinesin motors along microtubules by reversibly manipulating the properties of the neck of the human kinesin-1 and the heterodimeric kinesin-2 *Sp*KRP85/95 from sea urchin. The neck region of kinesin-1 was shown to form a stable coiled coil in solution (Huang et al., 1994; Morii et al., 1997; Tripet et al., 1997), and, as predicted, we found this motor to track one protofilament. A construct derived from this kinesin-1 containing flexible extensions introduced immediately after its neck linker indeed displayed pronounced left-handed spiraling around the microtubule. The final and most stringent test was to revoke the introduced flexibility by crosslinking that significantly reduced the motor's pitch up to the point of protofilament tracking, as predicted (Figure 5C, bottom traces). Similarly, the heterodimeric *Sp*KRP85/95 displayed a significantly reduced propensity to generate torque after introducing a chemical crosslink following its neck linker (Figure 6C). Because crosslinking right after the neck linker mimics a stable neck formation in double-headed kinesin motors, our data provide strong evidence that the propensity to generate torque is dictated by the structural integrity of the coiled coil in the neck region.

## Kinesin's Processivity versus Torque Generation

Earlier studies have suggested that the spiraling behavior of kinesins is directly linked to their processivity (Yajima et al., 2008). Yildiz et al. showed that human kinesin-1 constructs with and without the flexible extensions are both equally processive (Yildiz et al., 2008). Nevertheless, in our assays we detect single protofilament tracking with the kinesin-1 construct containing the wild-type neck, whereas the construct containing the flexible extensions displayed a pronounced left-handed spiraling around a suspended microtubule despite being similarly processive. Likewise, *Ce*KLP11/20 and *Mm*KIF3a/3b are similarly processive (Brunnbauer et al., 2010; Muthukrishnan et al., 2009), though the former generates considerable torque

**Table 1. Heterodimeric Kinesin-2 Constructs from Mouse, *X. laevis*, and Sea Urchin**

| Subunit | Tail Mutations |
|---|---|
| *Mm*KIF3a | G484E/G485E |
| *Mm*KIF3b | G477E/G478E |
| *Xl*KLP3a | G482E/G483E |
| *Xl*KLP3b | G477E/G478E |
| *Sp*KRP85 | G480E/G481E |
| *Sp*KRP95 | G474E/G475E |

whereas the latter moves torque-free along one protofilament. Finally, the processive *Ce*KLP11/20 kinesin-2 from *C. elegans* and its unprocessive counterpart KLP11/11 both displayed an equivalent pitch. Apparently, a direct correlation between processivity and torque generation cannot be established. Instead, our findings point to neck stability as the decisive factor for controlling the torque generation and protofilament switching. Support for this view comes from earlier studies where kinesin-1 constructs with neck extensions were shown to reach off-axis binding sites on the microtubule (Yildiz et al., 2008).

## Tuning Kinesin's Path on the Microtubule for Cellular Transport

So far, the examples of torque-generating kinesins were limited predominantly to (natural or artificial) unprocessive kinesins (Pan et al., 2010; Walker et al., 1990; Yajima and Cross, 2005; Yajima et al., 2008). The present work uncovers that numerous processive kinesins involved in cargo transport generate torque, too. In stark contrast to the processive kinesin-1, which strictly tracks one protofilament on the microtubule, these motors display an intrinsic and characteristic propensity to take side steps while they move on their filament.

In fact, spiraling movement of kinesin motors appears to be the rule rather than the exception: from the kinesin-2 motors tested, only the kinesin-2 from mouse was capable of tracking a single protofilament as does kinesin-1. Our findings thus extend the current understanding of force generation by kinesin motors and demonstrate that the torque-free cargo transport by kinesin-1 is a remarkable exception. This point is highlighted by our construct hCys-14GS-X. The flexibility introduced by the two additional lysine residues preceding the crosslinking site interferes with the ability of the motor to track just one protofilament.

What might the implications of this fundamental mechanistic property of side stepping be? Inside cells the surface of microtubules is crowded with associated proteins that are thought to hamper the unobstructed transport by molecular motors (Stamer et al., 2002). Intuitively, one might argue that the ability to take side steps has its advantages, as it may endow the motor molecules with the flexibility to evade macromolecular obstacles encountered in the linear path. However, very little is known about effects of molecular crowding on microtubules in vivo. Moreover, conflicting results have been reported for the behavior of kinesin-1 at "roadblocks" in vitro and in vivo (Cai et al., 2007; Seitz and Surrey, 2006; Telley et al., 2009). Future work will have to determine the significance of the propensity of molecular transporters to side step—or not to side step—during cargo transport.

## EXPERIMENTAL PROCEDURES

### DNA Constructs and Design

The following constructs were all cloned into the pFastBac1 vector (Invitrogen) using SpeI and NotI sites for the Baculovirus Expression System (Invitrogen). Constructs were made with a C-terminal Flag tag (F) or a 6X-Histidine tag (H) to facilitate protein purification.

#### *Kinesin-2 Constructs*

The design of the *C. elegans* kinesin-2 and its chimeric constructs are described elsewhere (Brunnbauer et al., 2010). The heterodimeric kinesin-2 constructs from mouse (*Mm*KIF3a-H, *Mm*KIF3b-F), sea urchin (*Sp*KRP85-F, *Sp*KRP95-H), and *X. laevis* (*Xl*KLP3a-F, *Xl*KLP3b-H) were custom synthesized by GenScript USA containing the glutamate point mutations in their tail domains as described (Brunnbauer et al., 2010) (Table 1).

#### *Mouse/C. elegans Chimeric Constructs*

To create the chimeric construct containing the mouse head and neck linker domains fused to the *C. elegans* kinesin-2 NST, the following splice sites were used (Figure 4A):

L359 (*Mm*KIF3a)/L346 (*Ce*KLP20)
L354 (*Mm*KIF3b)/L358 (*Ce*KLP11)

To create the chimeric construct containing the mouse head domain fused to the *C. elegans* kinesin-2 neck linker and NST domains, the following splice sites were used (Figure 4A):

I345 (*Mm*KIF3a)/Q332 (*Ce*KLP20)
I340 (*Mm*KIF3b)/K344 (*Ce*KLP11)

The following residues were swapped to exchange the neck linker of *C. elegans* kinesin-2 onto the mouse kinesin-2 (Figure 4):

K346 N K A R I N E D P K D A L (*Mm*KIF3a) exchanged with:
Q332 N V A K I N E D P K D A Q (*Ce*KLP20)
K341 N K P R V N E D P K D A L (*Mm*KIF3b) exchanged with:
K344 N Q P K I N E D P K D A L (*Ce*KLP11)

To ensure that no secondary mutations were introduced during the course of the cloning procedure, all three constructs were subjected to DNA sequencing.

#### *Human Kinesin-1, KIF-KLP-KIF, and hCys-SpKRP85/95 Kinesin-2 Constructs*

The cysteine-light human kinesin-1, hCys-*Sp*KRP85/95, and KIF-KLP-KIF constructs were custom synthesized by GenScript USA after Rice et al. (1999) and Yildiz et al. (2008), with alterations as highlighted in Figure 5A for kinesin-1, in Figure 6A for kinesin-2, and in Figure 4 for KIF-KLP-KIF.

### Protein Expression, Purification, and Crosslinking

All proteins were expressed and purified using the Baculovirus Expression System (Invitrogen) in insect cells (*Spodoptera frugiperda* [Sf9]) using the ANTI-FLAG M2 Affinity Agarose Gel (Sigma) against the C-terminal Flag-tag of the constructs as described (Brunnbauer et al., 2010). For the heterodimeric kinesin-2 constructs, protein purification using the ANTI-FLAG M2 Affinity Agarose Gel against the C-terminal Flag-tag of one subunit was sufficient to copurify its heterodimeric partner in a 1:1 ratio in all cases.

The following alterations in the purification protocol were made to enable cysteine-cysteine crosslinking in the kinesin-1 and kinesin-2 constructs containing the reactive cysteine residues (along with the respective control constructs) using the bis-functionalized cysteine-specific crosslinker $BM(PEG)_2$ (Thermo Scientific, Product-Number 22336): DTT in the wash and elution buffer was replaced with 0.5 mM TCEP. Proteins were reacted with the crosslinker in 1:1 molar ratio for 45 min at room temperature. The crosslinking reactions were quenched with 25 mM DTT, flash-frozen in liquid nitrogen immediately, and stored at −80°C. The specificity and efficiency of the reaction was assessed by SDS-PAGE.

### Optical Tweezers Setup and Sample Preparation

The setup of the optical tweezers is described (Brunnbauer et al., 2010; Gebhardt et al., 2010). The trapping laser is split in two beams with orthogonal polarization. One of the beams was passed through an AOD. The position control of the AOD by a DSP-board allowed rapid timesharing of this beam between two positions to generate the two steerable trapping potentials used to capture the pillar beads. The beads were monitored using a custom-built, integrated, inverted microscope. Bright-field images of the beads were recorded at a frame rate of 40 ms.

### Preparation of Motor-Bead Complexes

Desired amounts of protein were incubated with 1 μm diameter Polybead Carboxylate Microspheres (2.6%) or Polybead Polystyrene Microspheres (2.6%) as follows: 10 μl of preblocking buffer (80 mM PIPES [pH 6.9], 2 mM $MgCl_2$, 1 mM EGTA, 1 mM DTT, 0.1 mg/ml casein, 0.1 mg/ml cytochrome *c*,1 mM ATP) was mixed with 10 μl microspheres that was 5-fold diluted in 80 mM PIPES (pH 6.9), 2 mM $MgCl_2$, 1 mM EGTA, 1 mM DTT and incubated for 5 min on ice. Ten microliters of a protein dilution in 80 mM PIPES (pH 6.9), 2 mM $MgCl_2$, 1 mM EGTA, 1 mM DTT, 0.1 mg/ml casein was added to the preblocked beads and further incubated on ice for 5 min.

### Preparation of Motor-Antibody-Bead Complexes

Polybead amino microspheres (1 μm, 2.6%) were functionalized with glutaraldehyde as instructed by the manufacturer (Polysciences, Inc.). The microspheres were first coupled to excess Protein G, washed in PBS, and finally coupled to excess monoclonal anti-Flag antibody (Sigma). The final wash was done in 80 mM PIPES (pH 6.9), 2 mM $MgCl_2$, 1 mM EGTA, 1 mM DTT. Ten microliters of a protein dilution in 80 mM PIPES (pH 6.9), 2 mM $MgCl_2$, 1 mM EGTA, 1 mM DTT, 0.1 mg/ml casein was incubated with 10 μl of the anti-Flag antibody-functionalized microspheres on ice for 5 min.

### Preparation of the Flow Chambers

Ten microliters of the buffer (80 mM PIPES [pH 6.9], 2 mM $MgCl_2$, 1 mM EGTA, 1 mM DTT, 1 mg/ml BSA) was used to preblock the surface of the flow chamber. Desired amounts of Atto-488-labeled and biotinylated microtubules, 3 μm neutravidin-coated microspheres (Bangs Laboratories, Inc), and protein-coated 1 μm microspheres were added to 50 μl of motility buffer (80 mM PIPES [pH 6.9], 100 mM potassium acetate, 2 mM $MgCl_2$, 1 mM EGTA, 1 mM DTT, 1 mM ATP, 0.4% glucose, 0.145 mg/ml glucose oxidase [Sigma], 0.0485 mg/ml catalase [Sigma], 0.2 mg/ml casein) and flown into the chamber.

## SUPPLEMENTAL INFORMATION

Supplemental Information includes five figures, one table, Supplemental Discussion, and six movies and can be found with this article online at doi:10.1016/j.molcel.2012.04.005.

## ACKNOWLEDGMENTS

This work was supported by funds from Deutsche Forschungsgemeinschaft SFB863. We are indebted to Jonathan M. Scholey for discussions about unpublished results from his laboratory, which paved the way for this work. We would like to acknowledge Süleyman Kösem for providing microtubules of excellent quality and Felix Mueller-Planitz for discussions throughout the progress of this work and for critically reading the manuscript. We are especially grateful for little Benedikt Brunnbauer's constant smiling during the revision and to his babysitter Dr. Christine Wurm for being available at all times.

Received: September 29, 2011
Revised: February 23, 2012
Accepted: April 6, 2012
Published online: April 26, 2012

## REFERENCES

Ali, M.Y., Uemura, S., Adachi, K., Itoh, H., Kinosita, K., Jr., and Ishiwata, S. (2002). Myosin V is a left-handed spiral motor on the right-handed actin helix. Nat. Struct. Biol. *9*, 464–467.

Ali, M.Y., Homma, K., Iwane, A.H., Adachi, K., Itoh, H., Kinosita, K., Jr., Yanagida, T., and Ikebe, M. (2004). Unconstrained steps of myosin VI appear longest among known molecular motors. Biophys. J. *86*, 3804–3810.

Brunnbauer, M., Mueller-Planitz, F., Kösem, S., Ho, T.H., Dombi, R., Gebhardt, J.C., Rief, M., and Okten, Z. (2010). Regulation of a heterodimeric kinesin-2 through an unprocessive motor domain that is turned processive by its partner. Proc. Natl. Acad. Sci. USA *107*, 10460–10465.

Cai, D., Verhey, K.J., and Meyhöfer, E. (2007). Tracking single Kinesin molecules in the cytoplasm of mammalian cells. Biophys. J. *92*, 4137–4144.

Carter, N.J., and Cross, R.A. (2005). Mechanics of the kinesin step. Nature *435*, 308–312.

Chana, M.S., Tripet, B.P., Mant, C.T., and Hodges, R. (2005). Stability and specificity of heterodimer formation for the coiled-coil neck regions of the motor proteins Kif3A and Kif3B: the role of unstructured oppositely charged regions. J. Pept. Res. *65*, 209–220.

Chrétien, D., and Wade, R.H. (1991). New data on the microtubule surface lattice. Biol. Cell *71*, 161–174.

De Marco, V., Burkhard, P., Le Bot, N., Vernos, I., and Hoenger, A. (2001). Analysis of heterodimer formation by Xklp3A/B, a newly cloned kinesin-II from Xenopus laevis. EMBO J. *20*, 3370–3379.

Gebhardt, J.C., Bornschlögl, T., and Rief, M. (2010). Full distance-resolved folding energy landscape of one single protein molecule. Proc. Natl. Acad. Sci. USA *107*, 2013–2018.

Huang, T.G., Suhan, J., and Hackney, D.D. (1994). Drosophila kinesin motor domain extending to amino acid position 392 is dimeric when expressed in Escherichia coli. J. Biol. Chem. *269*, 16502–16507.

Imanishi, M., Endres, N.F., Gennerich, A., and Vale, R.D. (2006). Autoinhibition regulates the motility of the C. elegans intraflagellar transport motor OSM-3. J. Cell Biol. *174*, 931–937.

Kozielski, F., Sack, S., Marx, A., Thormählen, M., Schönbrunn, E., Biou, V., Thompson, A., Mandelkow, E.M., and Mandelkow, E. (1997). The crystal structure of dimeric kinesin and implications for microtubule-dependent motility. Cell *91*, 985–994.

Kural, C., Serpinskaya, A.S., Chou, Y.H., Goldman, R.D., Gelfand, V.I., and Selvin, P.R. (2007). Tracking melanosomes inside a cell to study molecular motors and their interaction. Proc. Natl. Acad. Sci. USA *104*, 5378–5382.

Mitchell, D.R. (2007). The evolution of eukaryotic cilia and flagella as motile and sensory organelles. Adv. Exp. Med. Biol. *607*, 130–140.

Morii, H., Takenawa, T., Arisaka, F., and Shimizu, T. (1997). Identification of kinesin neck region as a stable α-helical coiled coil and its thermodynamic characterization. Biochemistry *36*, 1933–1942.

Muthukrishnan, G., Zhang, Y., Shastry, S., and Hancock, W.O. (2009). The processivity of kinesin-2 motors suggests diminished front-head gating. Curr. Biol. *19*, 442–447.

Nishizaka, T., Yagi, T., Tanaka, Y., and Ishiwata, S. (1993). Right-handed rotation of an actin filament in an in vitro motile system. Nature *361*, 269–271.

Nitzsche, B., Ruhnow, F., and Diez, S. (2008). Quantum-dot-assisted characterization of microtubule rotations during cargo transport. Nat. Nanotechnol. *3*, 552–556.

Okten, Z., Churchman, L.S., Rock, R.S., and Spudich, J.A. (2004). Myosin VI walks hand-over-hand along actin. Nat. Struct. Mol. Biol. *11*, 884–887.

Pan, X., Acar, S., and Scholey, J.M. (2010). Torque generation by one of the motor subunits of heterotrimeric kinesin-2. Biochem. Biophys. Res. Commun. *401*, 53–57.

Pierce, D.W., Hom-Booher, N., Otsuka, A.J., and Vale, R.D. (1999). Single-molecule behavior of monomeric and heteromeric kinesins. Biochemistry *38*, 5412–5421.

Ray, S., Meyhöfer, E., Milligan, R.A., and Howard, J. (1993). Kinesin follows the microtubule's protofilament axis. J. Cell Biol. *121*, 1083–1093.

Reck-Peterson, S.L., Yildiz, A., Carter, A.P., Gennerich, A., Zhang, N., and Vale, R.D. (2006). Single-molecule analysis of dynein processivity and stepping behavior. Cell *126*, 335–348.

Rice, S.E. (2001). A structural change in the neck region of Kinesin motors drives unidirectional motility (San Francisco: Univ. of California).

Rice, S.E., Lin, A.W., Safer, D., Hart, C.L., Naber, N., Carragher, B.O., Cain, S.M., Pechatnikova, E., Wilson-Kubalek, E.M., Whittaker, M., et al. (1999). A structural change in the kinesin motor protein that drives motility. Nature *402*, 778–784.

Scholey, J.M. (2003). Intraflagellar transport. Annu. Rev. Cell Dev. Biol. *19*, 423–443.

Seitz, A., and Surrey, T. (2006). Processive movement of single kinesins on crowded microtubules visualized using quantum dots. EMBO J. *25*, 267–277.

Sindelar, C.V., and Downing, K.H. (2007). The beginning of kinesin's force-generating cycle visualized at 9-A resolution. J. Cell Biol. *177*, 377–385.

Sindelar, C.V., Budny, M.J., Rice, S.E., Naber, N., Fletterick, R., and Cooke, R. (2002). Two conformations in the human kinesin power stroke defined by X-ray crystallography and EPR spectroscopy. Nat. Struct. Biol. *9*, 844–848.

Stamer, K., Vogel, R., Thies, E., Mandelkow, E., and Mandelkow, E.M. (2002). Tau blocks traffic of organelles, neurofilaments, and APP vesicles in neurons and enhances oxidative stress. J. Cell Biol. *156*, 1051–1063.

Telley, I.A., Bieling, P., and Surrey, T. (2009). Obstacles on the microtubule reduce the processivity of Kinesin-1 in a minimal in vitro system and in cell extract. Biophys. J. *96*, 3341–3353.

Tilney, L.G., Bryan, J., Bush, D.J., Fujiwara, K., Mooseker, M.S., Murphy, D.B., and Snyder, D.H. (1973). Microtubules: evidence for 13 protofilaments. J. Cell Biol. *59*, 267–275.

Tripet, B., Vale, R.D., and Hodges, R.S. (1997). Demonstration of coiled-coil interactions within the kinesin neck region using synthetic peptides. Implications for motor activity. J. Biol. Chem. *272*, 8946–8956.

Tuma, M.C., Zill, A., Le Bot, N., Vernos, I., and Gelfand, V. (1998). Heterotrimeric kinesin II is the microtubule motor protein responsible for pigment dispersion in Xenopus melanophores. J. Cell Biol. *143*, 1547–1558.

Vale, R.D., and Toyoshima, Y.Y. (1988). Rotation and translocation of microtubules in vitro induced by dyneins from Tetrahymena cilia. Cell *52*, 459–469.

Valentine, M.T., Fordyce, P.M., Krzysiak, T.C., Gilbert, S.P., and Block, S.M. (2006). Individual dimers of the mitotic kinesin motor Eg5 step processively and support substantial loads in vitro. Nat. Cell Biol. *8*, 470–476.

Vukajlovic, M., Dietz, H., Schliwa, M., and Ökten, Z. (2011). How kinesin-2 forms a stalk. Mol. Biol. Cell *22*, 4279–4287.

Walker, R.A., Salmon, E.D., and Endow, S.A. (1990). The Drosophila claret segregation protein is a minus-end directed motor molecule. Nature *347*, 780–782.

Wedaman, K.P., Meyer, D.W., Rashid, D.J., Cole, D.G., and Scholey, J.M. (1996). Sequence and submolecular localization of the 115-kD accessory subunit of the heterotrimeric kinesin-II (KRP85/95) complex. J. Cell Biol. *132*, 371–380.

Yajima, J., and Cross, R.A. (2005). A torque component in the kinesin-1 power stroke. Nat. Chem. Biol. *1*, 338–341.

Yajima, J., Mizutani, K., and Nishizaka, T. (2008). A torque component present in mitotic kinesin Eg5 revealed by three-dimensional tracking. Nat. Struct. Mol. Biol. *15*, 1119–1121.

Yamazaki, H., Nakata, T., Okada, Y., and Hirokawa, N. (1995). KIF3A/B: a heterodimeric kinesin superfamily protein that works as a microtubule plus end-directed motor for membrane organelle transport. J. Cell Biol. *130*, 1387–1399.

Yamazaki, H., Nakata, T., Okada, Y., and Hirokawa, N. (1996). Cloning and characterization of KAP3: a novel kinesin superfamily-associated protein of KIF3A/3B. Proc. Natl. Acad. Sci. USA *93*, 8443–8448.

Yildiz, A., Tomishige, M., Gennerich, A., and Vale, R.D. (2008). Intramolecular strain coordinates kinesin stepping behavior along microtubules. Cell *134*, 1030–1041.